

# Microstructure evolution of granular soils during liquefaction process

Jiangtao Wei & Gang Wang

*Department of Civil and Environmental Engineering, The Hong Kong University of Science and Technology, Clear Water Bay, Hong Kong, China*

**ABSTRACT:** In this study, microstructure evolution of granular soils during liquefaction process is investigated using Discrete Element simulation. The granular packing is regarded as an assemblage of particles and voids. A new index, termed as Centroid Distance, is proposed to characterize the distribution of voids around the particles. The index is found to be effective to characterize the microstructure evolution of the granular packing during the cyclic mobility and post-liquefaction process. Using this index, various liquefaction behaviors of granular soils can be explained, including the progressive accumulation of shear deformations, occurrence of flow deformation and strain-hardening in the post-liquefaction stage.

## 1 INTRODUCTION

Liquefaction refers to the phenomenon related to the increase of pore water pressure in saturated sand under undrained cyclic loading such as earthquake loading. In the past, many laboratory cyclic triaxial tests and cyclic simple shear tests have been conducted to investigate the soil liquefaction. Most studies have been focused on the stress-strain behaviors and the influence of different factors on the liquefaction potential of granular soils, such as initial density, cyclic stress ratio (CSR), confining pressure and initial static shear stress etc. (Seed 1983, Vaid *et al.* 2001, Yang & Sze 2011). However, laboratory investigations can only measure the macroscopic soil behaviors. It is also difficult to interpret the microscopic behaviors of the soil response from the test results, as non-uniform stress and strain fields are often induced in the test samples.

In recent years, Discrete Element Method (DEM) has been widely used to study the micromechanical characteristics of soil behaviors, where particle-by-particle response of a granular assemblage can be closely examined by DEM simulation. Furthermore, any desired particle scale information at any time during the numerical test can be easily obtained. In dealing with the non-liquefiable soils, most micromechanical investigations are based on the information of particle contact (Rothenberg & Bathurst 1989, Radjai *et al.* 1998, Thornton 2000, Li *et al.* 2009). However, particle-contact based method only is not enough to deal with the liquefaction problem since the extremely low contact number during the flowing strain stage. In recent years, some research-

ers have studied the behaviors of liquefaction using DEM simulation. For example, Ng & Dobry (1994) verify the capability of DEM to simulate soil behavior under undrained cyclic loading. Ashmawy *et al.* (2003) evaluate the influence of particle shape on liquefaction potential. Sitharam *et al.* (2009) investigate the evolution of internal variables during post-liquefaction under undrained monotonic loading.

In this paper, a novel method in terms of particle position is developed. The microstructural evolution of the granular packing during the whole loading process is studied based on the method.

## 2 LIQUEFACTION SIMULATION BY DEM

In this study, an open source DEM code, Yade, is used to conduct the numerical simulations. 4,000 disk-shaped (2D) particles are randomly generated in a squared representative volume element (RVE). Periodic boundary is prescribed on this RVE to eliminate the non-uniformity caused by RVE boundary. The radius of particles ranges from 0.15mm to 0.45mm and the mean radius  $R_{50}$  is 0.3mm. A non-linear Hertz-Mindlin model was used to describe the particle contact behavior. The following material properties are assigned to all the particles: Young's modulus of 70GPa, Poisson's ratio of 0.3 and frictional coefficient of 0.5. Since the simulation is quasi-static, the density of particles is scaled by a factor of  $2 \times 10^5$  in order to reduce the computational time without affecting the solutions. After particles generation, the packing was isotropically consolidated to an initial confining pressure  $p=100$  kPa. Packings

with different void ratios can be obtained by specifying different particle frictional coefficients during the consolidation stage. Figure 1(a) shows the particle configuration with the void ratio of 0.228.

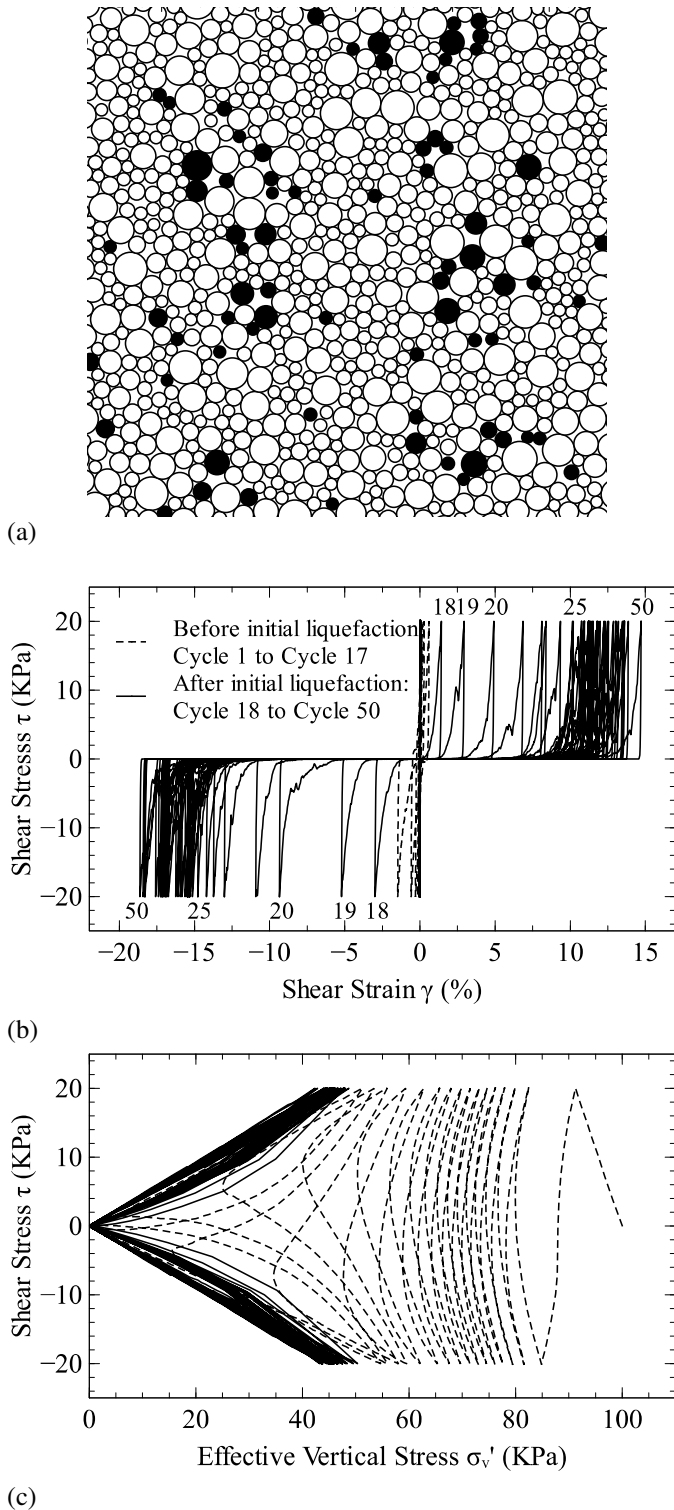


Figure 1. Macroscopic behavior of granular packing under undrained cyclic loading from DEM, (a) Particle configuration at the outset of cyclic loading (close-up view, not all particles are shown), (b) Shear stress and shear strain relation, (c) Shear stress and effective vertical stress relation

During undrained cyclic simple-shear test, a constant strain rate of 0.01/s was applied in order to ensure the quasi-static condition. The simulation was stress controlled with a cyclic stress ratio (CSR) of 0.2. During the simulation, the volume of RVE is

kept unchanged to ensure an undrained condition. The pore water pressure is determined by the difference between the vertical total stress and the vertical effective stress. Figure 1b shows the relationship between shear stress ( $\tau$ ) and shear strain ( $\gamma$ ). Figure 1c shows the evolution of shear stress ( $\tau$ ) with the effective vertical normal stress ( $\sigma_v'$ ). The soil sample reached initial liquefaction after 17 cycles, which is indicated by zero effective stress. The simulation result is qualitatively similar to the laboratory test results of a dense granular soil sample. Typical behaviors can be observed from the DEM simulation, such as the gradual decrease of effective vertical stress  $\sigma_v'$  in each load cycle till liquefaction, increase of shear strain  $\gamma$  with the number of load cycles, and phase transform from contraction to dilation in each load cycle. The maximum strain of each cycle before initial liquefaction increase very slowly and  $\gamma_{\max}$  of cycle 17 in which the initial liquefaction occurs is only 2.1%. From cycle 17 to cycle 25, the maximum strain increase dramatically. After cycle 25, the increasing rate of the maximum strain is slowing down. In the later part of the paper, this behavior will be discussed more specific.

### 3 MICROSTRUCTUE OF GRANULAR SOILS

#### 3.1 The definition of microstructural index

For granular soils, Voronoi cell can be conveniently used to divide the void space around each particle. As shown in Figure 2, the Voronoi cell for particle  $i$  is a convex polygon enclosed by  $C_1$ - $C_2$ - $C_3$ - $C_4$ - $C_5$ . The mass center of the Voronoi cell and the mass center of the particle are denoted as  $O^i$  and  $P^i$ , respectively. The centroid difference for particle  $i$  is defined as a vector:

$$\mathbf{D}^i = \frac{\mathbf{P}^i - \mathbf{O}^i}{R_{50}} \quad (1)$$

whose norm is defined as:

$$D_c^i = |\mathbf{D}^i| \quad (2)$$

where  $R_{50}$  is the mean particle radius of the granular packing. For each particle in the granular packing, its mobility is restricted by its surrounding particle. Centroid difference defined here is used to quantify the relation between the particle and its surrounding particles.

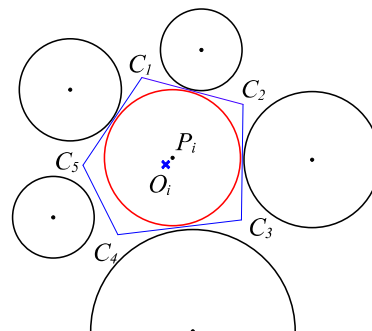


Figure 2. Schematic interpretation of Centroid Difference

The centroid distance ( $D_c$ ) of the whole packing can be defined as the average of  $D_c^i$  for all particles:

$$D_c = \frac{1}{N} \sum_i^N D_c^i \quad (3)$$

where  $N$  is the particle number. Figure 1a shows the particle configuration at the outset of the cyclic loading. The centroid distance of the packing  $D_c=0.0468$ . In this figure, solid particles with  $D_c^i \geq 2D_c$  are filled in solid color for easy identification. Relatively large pores can be found surrounding these solid particles. Therefore,  $D_c^i$  also represents the distribution of the void to some extent. Particles surrounded by relatively large pore have higher probability to have a larger value of  $D_c^i$ .

### 3.2 Probability density function of $D_c$

The probability density function of  $D_c$  for the granular packing before cyclic loading and during 50<sup>th</sup> loading cycle is illustrated in Figure 3. The figure shows that the proportion of large  $D_c$  corresponding to relatively large pores is decreasing during cyclic loading. Therefore the effect of undrained cyclic loading is to redistribute these relatively large pores. On the other hand, large pores would be occupied by particles and granular packing would be densified under a drained cyclic loading. Youd (1977) suggested the pore water pressure buildup of sands during cyclic loading is due to the collapse of the looser and more unstable arrays of particles within the sand. The evolution of probability density function supports Youd's suggestion.

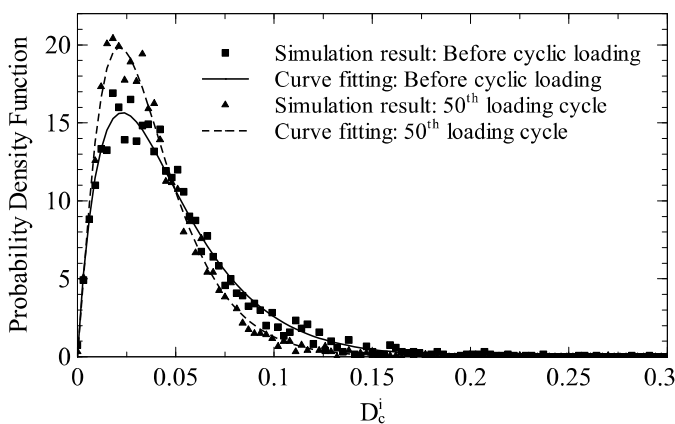


Figure 3. Probability density function of  $D_c$ . Gamma distribution is used to fit the curve

The presence of relatively large pores can be regarded as source of inhomogeneity in the granular packing. Due to the friction between granular particles and complex particle shape, local arching can be formed during the initial consolidation. The local arching preserves relatively large pores. Under the same stress condition, more relatively large pores

can be observed in the loose packing compared with a dense or medium packing. However, the arching structure is not stable and can be destroyed by the cyclic loading. Large pores are redistributed and the packing structure is more homogeneous as a result.

### 3.3 Evolution of $D_c$ and cyclic mobility

Figure 4 shows the evolution of  $D_c$  with the shear strain  $\gamma$  during 50 loading cycles. Before initial liquefaction, the change of  $D_c$  is very small. The most rapid decrease of  $D_c$  is experienced from cycle 17 to cycle 25. After the 25<sup>th</sup> cycle,  $D_c$  repeatedly increases and decreases within a loading cycle, with a net effect that  $D_c$  is reduced at the end of the cycle; however the decreasing rate gradually slows down. After approximately 30 loading cycles,  $D_c$  reaches a lower-bound limit. The evolution of  $D_c$  between different cycles is almost identical thereafter as shown in Figure 4.

The change of  $D_c$  can be regarded as a reflection of the packing structure adjustment (redistribution of the relatively large pores). Based on the evolution of  $D_c$ , it is possible to visualize the microscopic behavior of the granular packing during the stress-controlled cyclic loading. Within the first several cycles, the soil has not reached liquefaction stage. Very little change in the microstructure of the packing can be observed. However, even such little structure change will cause the mean effective stress to decrease until initial liquefaction occurs. Adjustment of the microstructure mainly happens within the post-liquefaction stage, especially during the first several cycles after the initial liquefaction.

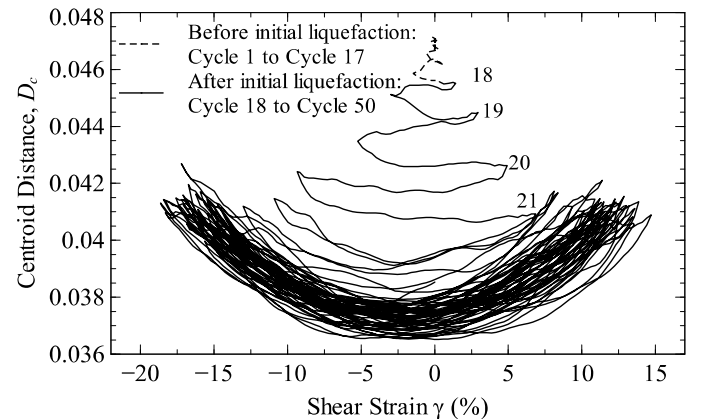


Figure 4. Evolution  $D_c$  during 50 loading cycles

In a stress-controlled cyclic simple shear test, the maximum strain developed in the soil continues to accumulate with increasing number of cycles, which is regarded as the cyclic mobility (cf. Fig. 1b). Through the DEM simulation, we observed that the cyclic mobility of the granular packing is strongly correlated to the evolution of  $D_c$ . Here, we use  $\gamma_c$  to measure the mobilized maximum shear strain in each load cycle ( $\gamma_c$  is the summation of maximum

shear strain in two directions). The relation between  $\gamma_c$  and  $D_c$  is demonstrated in Figure 5, where  $D_{c,min}$  in the figure refers to the minimum value attained within a loading cycle. Interestingly, significant change of  $D_c$  and  $\gamma_c$  occurs from cycle 17 (the initial liquefaction) to cycle 25. When  $D_{c,min}$  reaches to its lower-bound limit, the mobilized maximum shear strain  $\gamma_c$  also stabilizes around a constant value. The mobilized maximum shear strain ceases to increase under further loading cycles, and the stress-strain behavior of the soil is stabilized. It implies that the mobilized maximum shear strain during post-liquefaction stage is closely related to the packing configuration.

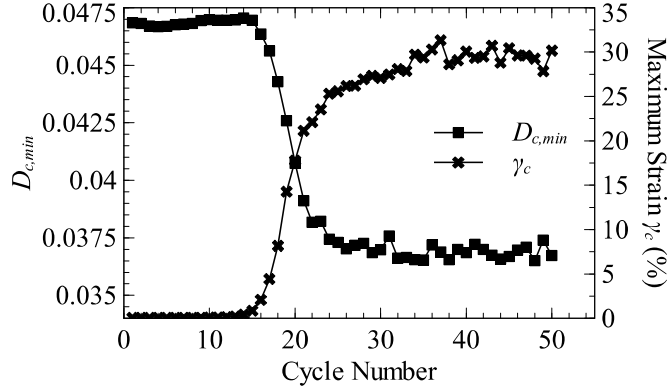


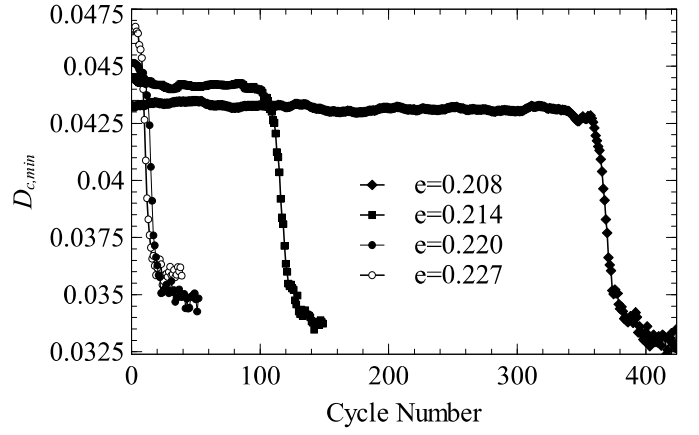
Figure 5. Relation between  $D_{c,min}$  and  $\gamma_c$

### 3.4 The decreasing trend of $D_{c,min}$

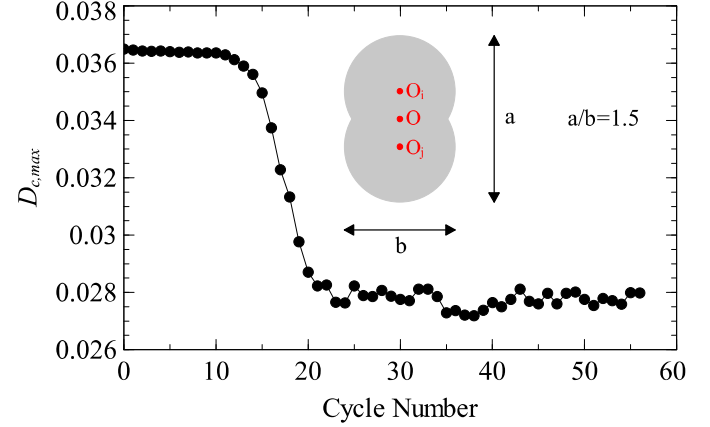
The decreasing trend of  $D_{c,min}$  during the cyclic loading is one of the most important properties since it has explicit physical interpretation, i.e., the redistribution and reduction of relatively large pores to smaller pores during cyclic loading.

The decreasing trend can be universally observed from all cyclic simple shear simulations we have conducted on samples with different densities and different particle shapes. Parts of simulation results are shown in Figure 6. Figure 6a demonstrates the density effect on the  $D_{c,min}$  evolution. Samples with a higher density (i.e., a smaller void ratio) will have a lower initial and final  $D_{c,min}$ . From the figure, we can also obtain the cycle number needed for the packing to liquefy. Packing with higher density need more cycles to liquefy, which is consistent with the laboratory test results.

Figure 6b demonstrates the result of the simulation using “peanut” shaped particles. It is to be noted that the shape effect on the liquefaction potential and on the change of  $D_{c,min}$  is not the emphasis of this paper. Again, a similar decreasing trend of  $D_{c,min}$  can be observed, implying that the trend is not affected by the particle shape.



(a)



(b)

Figure 6. (a) Evolution of  $D_c$  with different void ratio using disk particles; (b) Evolution of  $D_c$  with “peanut” shaped particle

### 3.5 The angular distribution of Centroid Difference in post-liquefaction stage

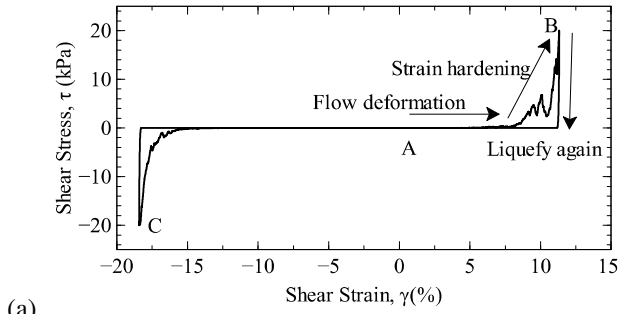
After initial liquefaction, the soil experiences flow deformation and then followed by strain hardening upon loading, when the sample can sustain considerable shear load. However, after stress reversal, the soil immediately liquefies. Figure 7(a) illustrates the stress-strain relationship in the 50<sup>th</sup> cycle. Figure 7(b) shows considerable variation of  $D_c$  during the loading, unloading and reloading process.

Since  $D_c$  is a scalar quantity averaged over the whole sample, it does not carry any information regarding the anisotropic re-distribution of the void during the post-liquefaction process. Following the method developed for the particle contact orientation (Rothenberg & Bathurst 1989), orientations of  $D_c$  can be characterized by an angular distribution function  $d_c(\theta)$ , which defines the averaged value of  $D_c^i$  in  $\theta$  direction within an angular interval of  $\Delta\theta$ .

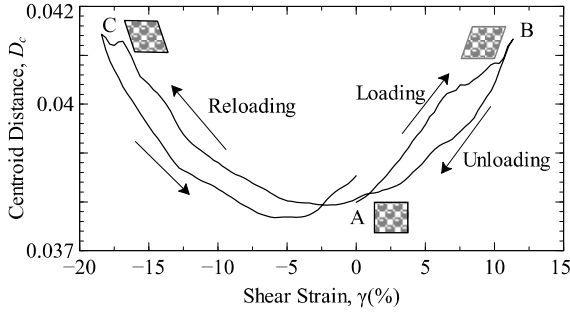
$$d_c(\theta) = \frac{1}{N\Delta\theta} \sum_{\theta^i \in [\theta, \theta + \Delta\theta]} D_c^i \quad (4)$$

Following the above definition and Eq. (3), it is obvious that

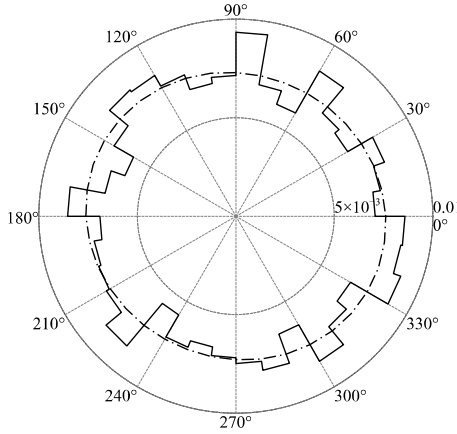
$$\int_0^{2\pi} d_c(\theta) d\theta = D_c \quad (5)$$



(a)



(b)

Figure 7. (a) Stress-strain relationship; (b) Evolution of  $D_c$  in the 50<sup>th</sup> loading cycle.Figure 8. The angular distribution of  $d_c(\theta)$  at the initial stage

For the two dimension case,  $d_c(\theta)$  can be approximated by the Fourier expression:

$$d_c(\theta) = \bar{d}_c [1 + a_c \cos 2(\theta - \theta_c)] \quad (6)$$

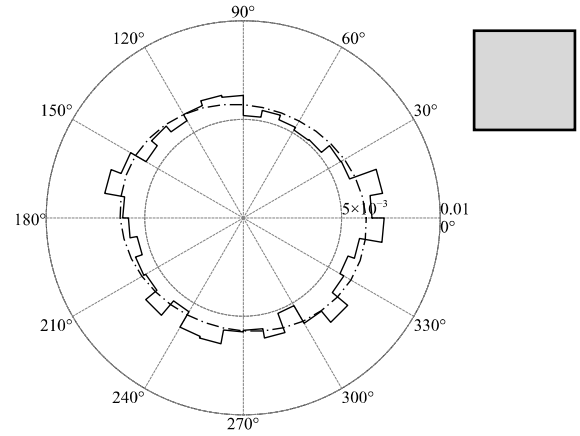
Here  $a_c$  is a parameter defining the magnitude of anisotropy and  $\theta_c$  defines the major principal direction.  $\bar{d}_c$  reflects the average of centroid distance over all particles and the relation between  $\bar{d}_c$  and  $D_c$ :

$$\bar{d}_c = \frac{D_c}{2\pi} \quad (7)$$

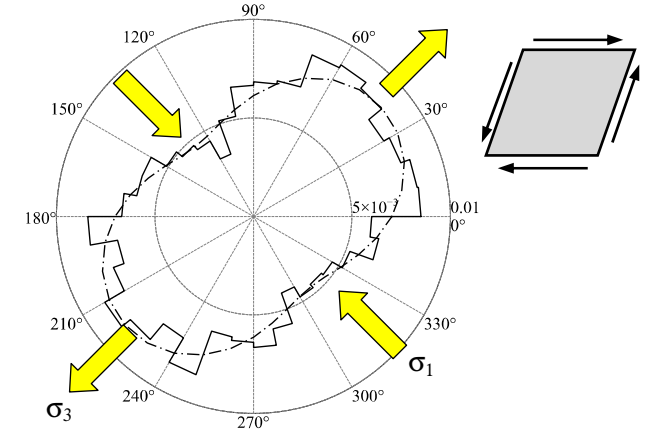
The polar histogram in Figure 8 demonstrates the angular distribution  $d_c(\theta)$  of the initial state of the packing (unliquefied, refer to Fig. 1a). The dash-dot line in the Figure 8 is the fitted Fourier form with  $\bar{d}_c = 7.45 \times 10^{-3}$ ,  $a_c = 0.033$ . The magnitude of anisotropy is so small that the angular distribution is nearly isotropic.

In the post-liquefaction stage, the angular distribution  $d_c(\theta)$  varies within a loading cycle. Referring

to Figure 7b,  $D_c$  peaks up from state A ( $\gamma=0\%$ ) to state B ( $\gamma=11.3\%$ ). The angular distributions  $d_c(\theta)$  for state A and B are demonstrated in Figure 9. At the fully liquefied state A, the angular distribution  $d_c(\theta)$  is almost isotropic, which is similar to the unliquefied initial state except that the radius of the circle is smaller than that of the initial state. At state B, the angular distribution  $d_c(\theta)$  is highly anisotropic with the magnitude of anisotropy  $a_c=0.3$ . The major principal direction of anisotropy is in line with the minor principal stress  $\sigma_3$  direction.



(a) Point A, fully liquefied state



(b) Point B, straining hardening state

Figure 9. The angular distribution of  $d_c(\theta)$  at different states, (a) Point A, (b) Point B at the 50<sup>th</sup> cycle

Figure 10 demonstrates the particle configuration and force chain of the packing at point B. Let  $\mathbf{n}_1$  be the major principal stress ( $\sigma_1$ , in compression) direction, and  $\mathbf{n}_3$  the minor principal stress ( $\sigma_3$ , in tension) directions. At state B, most strong force chains are located along  $\mathbf{n}_1$  direction with relatively large pores on either side. In the previous discussion, we have mentioned that the initial relatively large pores would be redistributed by cyclic loading. Similarly, shear deformation could also reorganize relatively large pores when the packing is upon loading from A to B. The reorganized large pores are not distributed randomly. Rather, relative to a soil particle, the relatively large pore has higher possibility to be located along  $\mathbf{n}_3$  direction due to tension in that direc-

tion. As a result,  $d_c(\theta)$  is highly anisotropic, with the maximum value attained in the tension direction ( $\mathbf{n}_3$ ), and minimum value in the compression direction ( $\mathbf{n}_1$ ), as shown in figure 9b. During the unloading process, the load is reversed and the compression load is applied in  $\mathbf{n}_3$  direction. Strong force chains cannot be organized in  $\mathbf{n}_3$  direction immediately upon the stress reversal. Instead, the packing would return to liquefaction state and experience flow deformation. These relatively large pores will be redistributed again until new strong force chains are formed in  $\mathbf{n}_3$  direction in the reloading process.

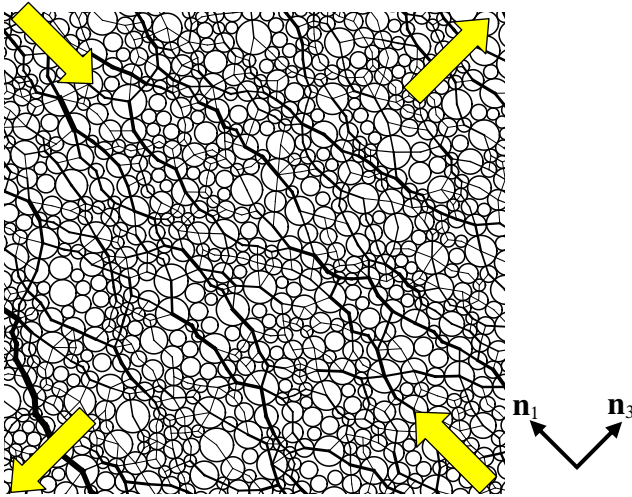


Figure 10. Particle configuration and force chain of the packing at state B

## 4 CONCLUSIONS

In this paper, numerical experiments are conducted to investigate the liquefaction behaviors of granular soils under undrained cyclic loading using DEM. The granular packing is regarded as an assemblage of particles and voids. The difference between the particle center and the Voronoi cell center is defined as “centroid distance” ( $D_c$ ). Physically,  $D_c$  reflects the distribution of void around the particles. Particles with relatively large pores around have higher probability to have large value of  $D_c$ . The index is found to be effective to characterize the microstructure of the granular packing during the cyclic mobility and post-liquefaction process.

It is worth pointing out that the proposed microstructure index is independent of particle contact. This feature is important to analyze microstructure evolution of the granular packing during liquefaction process, where zero effective stress would occur and therefore the contact number will decrease dramatically. Any microstructural analyses solely based on particle contacts are helpless in this case.

Using  $D_c$  as an indicator, the following microstructure evolution are observed during undrained cyclic loading:

- (a) The number of particles with a large value of  $D_c$  decreases during undrained cyclic loading, reflecting the redistribution of relatively large pores. The probability density function of  $D_c$  can be fitted by the gamma distribution.
- (b) The  $D_c$  of the whole packing decreases with increasing number of cycles. After sufficient cycles,  $D_c$  will reach to a lower-bound limit. Meanwhile, the mobilized maximum shear strain also stops increasing and is stabilized around a constant value. It is observed that cyclic mobility of the granular packing is strongly correlated to the evolution of
- (c) Highly anisotropic angular distribution of  $D_c$  is observed during the post-liquefaction stage, implying a special particle-void structure is formed.

The micromechanical study can provide significant insight to understand the liquefaction process. Although two-dimensional DEM simulations are conducted in this study, similar behaviors would be expected in 3D simulations, which will be conducted in the future.

## 5 ACKNOWLEDGEMENTS

The study was financially supported by RGC grant 620311 and DAG08/09EG01.

## 6 REFERENCES

- Ashmawy, A.K., Sukumaran, B. & Hoang, V.V. 2003. Evaluating the Influence of Particle Shape on Liquefaction Behavior Using Discrete Element Modeling. *Proc. 13th Int. Off-shore and Polar Engineering Conference*, 542-549
- Li, X., Yu, H.S. & Li, X.S. 2009. Macro-micro relations in granular mechanics. *International Journal of Solids and Structures* 46: 4331-4341.
- Ng, T.T. & Dobry, R. 1994. Numerical simulations of monotonic and cyclic loading of granular soil. *Journal of Geotechnical Engineering* 120(2): 388-403.
- Radjai, F., Wolf, D.E., Jean, M. & Moreau, J.J. 1998. Bimodal character of stress transmission in granular packings. *Physical Review Letter* 80: 61-64.
- Rothenburg, L. & Bathurst, R.J. 1989. Analytical study of induced anisotropy in idealized granular materials. *Geotechnique* 39(4): 601-14.
- Seed, H.B. 1983. Earthquake resistant design of earth dams. In *Proceeding, Symposium on Seismic Design of Embankments and Caverns*, Pennsylvania. ASCE, NY, pp. 41-64.
- Sitharam, T.G., Vinod, J.S. & Ravishankar, B.V. 2009. Post-liquefaction undrained monotonic behavior of sands: experiments and DEM simulations. *Geotechnique* 59(9): 739-749
- Thornton, C. 2000. Numerical simulations of deviatoric shear deformation of granular media. *Geotechnique* 50(1): 43-53.
- Vaid, Y.P., Stedman, J.D. & Sivathayalan S. 2001. Confining stress and static shear effects in cyclic liquefaction. *Canadian Geotechnical Journal* 38(3): 580-591
- Yang, J. & Sze, H.Y. 2011. Cyclic behaviour and resistance of saturated sand under non-symmetrical loading conditions. *Geotechnique* 61(1): 59-73
- Youd, T.L. 1977. Packing changes and liquefaction susceptibility. *Journal of the Geotechnical Engineering Division* 103(8): 918-922